ELSEVIER

Journal of Molecular Catalysis A: Chemical 119 (1997) 113–123

JOURNAL OF MOLECULAR CATALYSIS A: CHEMICAL

Two simple models for computer simulation of self-assembled monolayers

Michael Grunze *, Alexander J. Pertsin

Angewandte Physikalische Chemie am Physikalisch-Chemischen Institut der Universität Heidelberg, Im Neuenheimer Feld 253, D-69120 Heidelberg, FRG

Received 29 June 1996; accepted 17 October 1996

Abstract

To avoid computational difficulties involved in atomistic simulations of self-assembled monolayers (SAMs), two simple generalized models are suggested. One model deals with one-center particles representing headgroups and treats the interaction of the molecular tails in an implicit way, in terms of an effective one-center potential for the headgroup–headgroup interactions. In the other model, the interaction of the molecular tails is described explicitly using an orientation-dependent anisotropic potential function. Both the models include a surface corrugation potential responsible for the headgroup–substrate interactions. The form and parameters of the model potentials are chosen so as to mimic the interactions in alkanethiol/Au(111) SAMs. The phase and structural behavior of the model systems is studied as a function of temperature and coverage.

Keywords: Self-assembled monolayers; Monte Carlo simulation; Phase behavior

1. Introduction

Self-assembled monolayers (SAMs) which form by chemisorption of long-chain functionalized molecules onto the surface of solid substrates have received considerable attention in the last years. This attention is stimulated, on one hand, by diverse potential applications of SAMs and, on the other hand, by an intriguing phase behavior exhibited by these monolayer systems. Typical and best characterized examples of SAMs are monolayers of alkanethiols chemisorbed on a gold (111) surface [1] (hereafter, C_nS/Au(111) SAMs). At low temperatures and high coverages, the C_nS/Au(111) SAMs adopt a slightly distorted commensurate $(\sqrt{3} \times \sqrt{3})R30°$ triangular structure with the alkane tails tilted by $30 \pm 10°$ from the surface normal. With increasing temperature, the SAMs experience 2D structural transformations which are associated with a commensurate–incommensurate solid phase transition followed by 2D melting [2,3]. At low coverages, an interesting two-phase state is observed, in which the usual solid phase of tilted chains coexists with a so-called 'striped' phase. The structure proposed for the striped phase involves linear head-to-head dimers of alkanethiol molecules lying on the substrate surface parallel to each other [4].

* Corresponding author.

PII S1381-1169(96)00475-X

To understand the structure and phase behavior of $C_nS/Au(111)$ SAMs at the molecular level, a number of computer simulations have been made [5–8]. In all the cases, the molecular assembly was simulated using atomistic models [9], which treat each constituent atom (or, at least, each non-hydrogen atom) as a center of mass and force. Unfortunately, atomistic simulations are computationally too expensive to explore the phase behavior of SAMs in more or less detail. Thus, even for a medium-sized system of 224 molecules (the largest SAM system studied so far), the calculation of a single state point in the phase diagram took more than three months of c.p.u. time [8]. Simulations of small systems ($N < 100$) [6,7] are more feasible but hardly reliable because the size of such systems is comparable to the length of their constituent particles. Further difficulties arise from a high dimensionality of the configurational space of atomistic models, which may lead to ergodic problems [10] in simulation of dense crystal-like structures typical of SAMs.

In view of the problems involved in atomistic simulations, it seems reasonable, along with further developing the atomistic approach, to try simple generalized models, which reflect only dominant features of SAMs, while neglecting their atomistic details. In this paper we suggest two such models and explore their phase behavior as a function of temperature and coverage using the Monte Carlo technique. It is shown that simple generalized models, although useless in determination of the detailed structure of SAMs, may be of great utility in understanding, at the qualitative level, the essential physics underlying the SAM phase.

2. Models

As a zeroth-approximation model, we consider a 2D system of one-center particles representing headgroups, which interact with themselves via a pairwise isotropic potential and with the substrate via a periodic 'surface corrugation' potential. In this model, hereafter referred to as model 1, the chain–chain interactions are treated in an implicit form, through the use of a certain effective potential for the headgroup–headgroup interactions [11]. To find an appropriate effective potential, let us consider two interacting long-chain molecules standing perpendicular to the surface. If the spacing r between the molecular headgroups is increased while retaining the perpendicular molecular orientation, the distance dependence of the intermolecular interaction energy will look like a Lennard–Jones (6–12) potential. However, if the molecular orientations are allowed to change and the spacing between the molecular headgroups is again increased, the molecular tails will tilt so as to minimize the interaction energy and to retain the interchain spacing close to its equilibrium value, r_m. In this case the interaction energy will decrease nearly proportionally to the length of the 'overlapping' parts of the molecules, i.e. much slower compared to the inverse sixth power distance dependence characteristic of the Lennard–Jones potential. A slow distance dependence at $r > r_m$ is an important feature which allows the headgroups to accommodate the substrate lattice without substantial loss in energy.

The particular effective potential used in this work was derived from atomistic calculations of the static lattice energy of a substrate-free $C_{10}S/Au(111)$ SAM as a function of the monolayer lattice spacing [11]. For each given value of the lattice spacing, the alkanethiol chains were allowed to change their tilt, precession, and twist angles so as to minimize the lattice energy. Inasmuch as the interaction forces between alkanethiol molecules are essentially short-range, the lattice energy was mainly determined by the nearest neighbor interactions, so that the resulting dependence of the lattice energy on the lattice spacing offered just the effective potential of interest (accurate to a constant factor). After truncation at a cutoff distance $r_c = 1.6r_m$ and subsequent smoothing, the effective potential assumed a form which could be

well fitted with a linear combination of power and inverse power functions

$$\phi(r) = -1.03 + 0.072r^{8} - 0.0073r^{12} - 0.157r^{-16} + 0.125r^{-24} \quad (r < 1.6) \tag{1}$$

In this equation, $\phi(r)$ is given in a reduced form, with the potential well depth ε and equilibrium separation r_m taken as units of energy and distance. The absolute values of ε and r_m found from the lattice energy calculations on the $C_{10}S/Au(111)$ SAM were 6 kcal/mol and 4.4 Å, respectively.

The surface corrugation potential was taken in the form

$$(\phi)(\boldsymbol{r}) = b\left[3 - \sum_{k=1}^{3} \cos(\boldsymbol{r}\cdot\boldsymbol{g}_k)\right]/4.5, \tag{2}$$

where b has the meaning of the peak-to-valley roughness of the surface. In the calculations described in this article, b was treated as a variable parameter to follow the modulation effect of the substrate on the monolayer structure. The substrate reciprocal lattice vectors $\boldsymbol{g}_k$ in Eq. (3) were: $\boldsymbol{g}_1 = g_0(1, 0)$, $\boldsymbol{g}_2 = g_0(-\frac{1}{2}, \frac{\sqrt{3}}{2})$, $\boldsymbol{g}_3 = g_0(-\frac{1}{2}, -\frac{\sqrt{3}}{2})$ with $g_0 = 4\pi/\sqrt{3}\,c$. The value of $\sqrt{3}\,c$ was taken equal to 1.14, which corresponds to the relation observed in the $C_{10}S/Au(111)$ SAM ($\sqrt{3}\,c = 5.01$ Å and $r_m = 4.4$ Å).

In model 2, the orientational degrees of freedom of an alkanethiol molecule were treated in an explicit way. In this model each interacting molecule was represented by two force centers. One force center was placed at the headgroup and was not allowed to leave the plane of the substrate surface. This force center was responsible for the headgroup–substrate interactions and the associated interaction potential was assumed to have the same form as given by Eq. (4). The other force center was located in the middle of the chain and was responsible for the chain–chain and chain–substrate interactions. The interactions between the molecular chains were treated using an orientation-dependent 'ellipsoidal' generalization of the Lennard–Jones potential [12,13]

$$\Phi(\boldsymbol{u}_i, \boldsymbol{u}_j, \rho) = \varepsilon(\boldsymbol{u}_i, \boldsymbol{u}_j)\left\{\left[r - r_m(\boldsymbol{u}_i, \boldsymbol{u}_j, \rho) + 1\right]^{-12} - 2\left[r - r_m(\boldsymbol{u}_i, \boldsymbol{u}_j, \rho) + 1\right]^{-6}\right\}, \tag{3}$$

where $\boldsymbol{u}_i$ and $\boldsymbol{u}_j$ are unit vectors specifying the orientations of the interacting chains and ρ is the unit vector between their centers. If the equilibrium separation for the side-by-side parallel configuration ($\boldsymbol{u}_i\cdot\boldsymbol{u}_j = 1$, $\rho\cdot\boldsymbol{u}_i = \rho\cdot\boldsymbol{u}_j = 0$) is taken as the unit of distance, the equation for $r_m(\boldsymbol{u}_i, \boldsymbol{u}_j, \rho)$ assumes the form

$$r_m(\boldsymbol{u}_i, \boldsymbol{u}_j, \rho) = \left\{1 - \frac{a}{2}\left[\frac{(\rho\cdot\boldsymbol{u}_i + \rho\cdot\boldsymbol{u}_j)^2}{1 + a(\boldsymbol{u}_i\cdot\boldsymbol{u}_j)} + \frac{(\rho\cdot\boldsymbol{u}_i - \rho\cdot\boldsymbol{u}_j)^2}{1 - a(\boldsymbol{u}_i\cdot\boldsymbol{u}_j)}\right]\right\}^{-1/2}. \tag{4}$$

In this equation a is an anisotropy parameter defined by

$$a = (r_{ml}^2 - 1)/(r_{ml}^2 + 1), \tag{5}$$

where r_{ml} is the equilibrium chain–chain separation for the end-by-end linear configuration ($\boldsymbol{u}_i\cdot\boldsymbol{u}_j = \rho\cdot\boldsymbol{u}_j = 1$). In our calculations, r_{ml} was taken equal to 4, which approximately corresponds (in reduced units) to the length of $C_{10}S$ molecule. The well depth ε in Eq. (3) was assumed to have the form [12]

$$\varepsilon(\boldsymbol{u}_i, \boldsymbol{u}_j) = \left\{\left[1 - a^2(\boldsymbol{u}_i\cdot\boldsymbol{u}_j)^2\right]/(1 - a^2)\right\}^{-1/2}. \tag{6}$$

The interaction of the force center in the middle of the chain with the substrate was described by a 12-3 potential [6] dependent only on the distance z from the surface (i.e. the

second force center felt the surface as being absolutely smooth):

$$\psi(z) = \varepsilon_z\left[(z+1)^{-12} - 4(z+1)^{-3}\right]/3. \quad (7)$$

This potential has a minimum at $z = 0$ with a depth ε_z. For ε_z several values were tried between 0 and 3. Most calculations were performed with $\varepsilon_z = 1$, that is the potential wells for the chain–chain and chain–substrate interactions were assumed to be of the same depth.

The phase behavior of the model systems was simulated using the constant-NVT MC technique and periodic boundary conditions. A typical length of the MC run was $2 \cdot 10^5$ to $1 \cdot 10^6$ MC cycles. The number of particles in the periodic box, N, was taken equal to 504 and 576 for models 1 and 2, respectively. To see the dependence of the calculation results on the system size, several state points near the phase boundaries were recalculated with $N = 2016$ for model 1 and $N = 1296$ for model 2. The increase in the system size resulted only in slight shifts of the phase boundaries, whereas the qualitative phase behavior remained unchanged.

The structure and phase state of the model systems were monitored using various order parameters and correlation functions usually employed in simulations of 2D systems [14]. The extent of correlation between the arrangement of the headgroups and the substrate lattice was estimated in terms of the mean value, $\langle s \rangle$, r.m.s. fluctuation, $\sigma(s) = \sqrt{\langle s^2 \rangle - \langle s \rangle^2}$, and distribution of the local substrate-modulated translational order parameter s,

$$s = \frac{1}{m}\sum_{j=1}^{m}\frac{1}{3}\sum_{k=1}^{3}\cos(\boldsymbol{r}_j \cdot \boldsymbol{g}_k), \quad (8)$$

where the sum on j is over a cluster of m particles containing an arbitrarily picked particle and its nearest neighbors (most usually, $m = 7$).

All thermodynamic and structural quantities were evaluated using dimensionless reduced units defined in terms of ε and r_m [15]. The reduced area of the system was defined with reference to the substrate-free ground-state hexagonal structure, i.e. $A = A_{abs}/Nr_m^2\sqrt{3}/2$, where A_{abs} is the absolute area. Note that $A = (1.14)^2 = 1.3$ corresponds to the case when the number of particles in the system and the number of available adsorption sites on the substrate lattice are related as 1:3. This is the highest occupancy of adsorption sites that can be achieved when r_m is close to $\sqrt{3}\,c$, as is the case with our models.

3. Results and discussion

The phase behavior of the model 1 system was studied along some selected isotherms and isochores in the range $0.2 \leq T \leq 1$ and $0.9 < A < 1.8$, while the magnitude of surface corrugation, b, was varied from 0 to 1. The effect of b on the phase state of the system is illustrated in Fig. 1, which shows the T–b phase diagram at $A = 1.47$. In this diagram, S, L, and G refer to solid, liquid, and gas, respectively, while subscripts i and c at S are used to distinguish between commensurate and incommensurate solids. The S–L phase boundaries were located based mainly on changes in the long-range behavior of radial distribution functions [14]. Further indications of melting were provided by the r.m.s. displacement of particles and by the heat capacity c_v. The former became dependent on the length of the MC run and rapidly increased when related to a fixed number of MC cycles. The latter showed a peak whose height was generally 2–3 times greater than the average level of c_v far from the transition region. The appearance of gas in coexistence with solid or liquid was detected from the behavior of the r.m.s. fluctuation of density, which increased dramatically in the coexistence regions. Quantitatively, the two-phase regions involving gas could be readily identified from the snapshots of the system.

The most interesting property of the model 1 system was its ability to experience an incommensurate–commensurate solid phase transi-

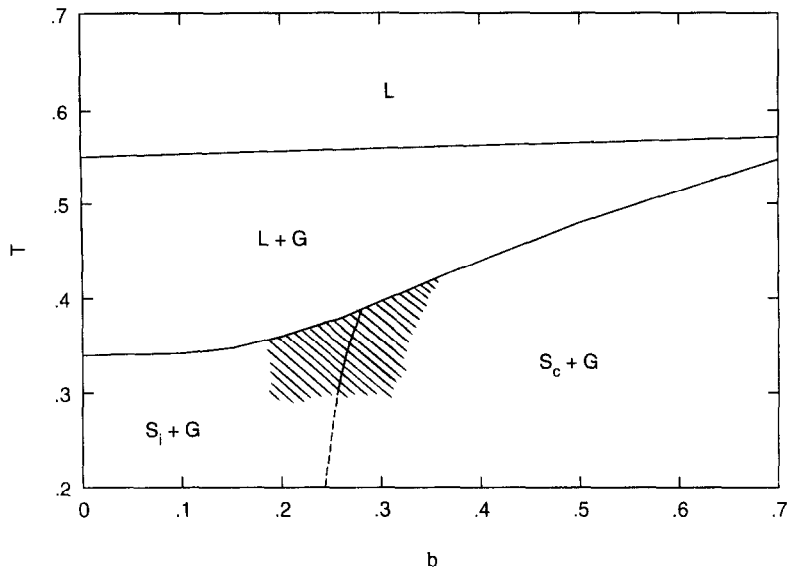

Fig. 1. The T–b phase diagram of the model 1 system at $A = 1.47$. The shaded area indicates the S_iS_c transition region. At $T < 0.3$, the exact location of the S_i–S_c phase boundary involved difficulties because of ergodic problems.

tion. This transition can well be seen from the evolution of the local substrate-modulated translational order parameter s as a function of corrugation b (Fig. 2). At $b = 0$, the distribution of s was, as expected, symmetric and centered at $s = 0$, so that $\langle s \rangle$ vanished. With increasing b to 0.1, a wing on the side of higher s appeared, so that $\langle s \rangle$ increased to about 0.07. The relevant snapshots, however, still showed no detectable changes because the increase in $\langle s \rangle$ was realized at the expense of subtle distortions in the original substrate-free crystal structure

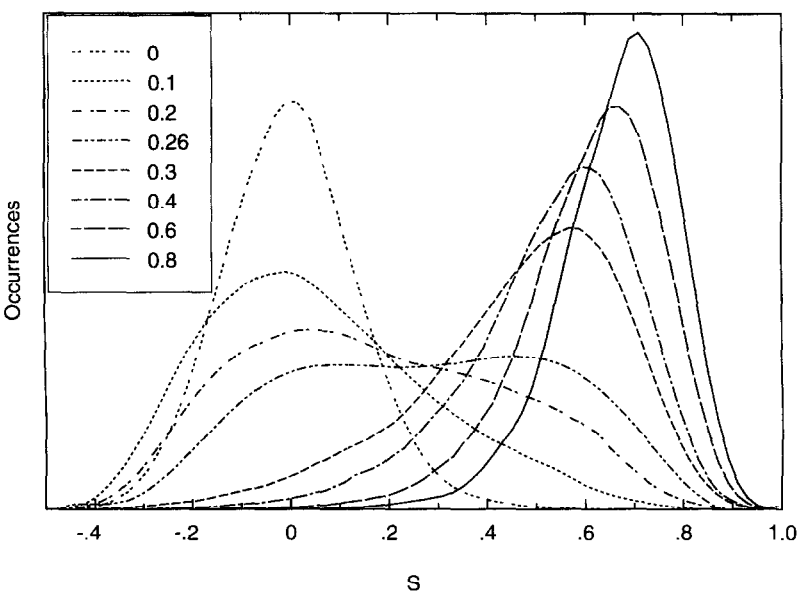

Fig. 2. Distribution of occurrences of the local substrate-modulated order parameter s in the model 1 system for different corrugations b at $T = 0.3$ and $A = 1.47$.

(Fig. 3a). Only at $b = 0.2$, the effect of the substrate could be revealed visually as the presence of domains with a clear substrate modulated local order (Fig. 3b). As b was further increased and passed a value of 0.26, the structure became 'mostly commensurate'.

It is important that the evolution of the distribution curves in Fig. 2 can be described fairly well in terms of a linear combination of two separate peaks, one at $s = 0$, corresponding to a substrate-free system state, and the other at $s = 0.5$–0.7, corresponding to a substrate modulated commensurate crystal structure. (A particularly illustrative case is at $b = 0.26$, when the two peaks are nearly equal in intensity). That is, for a rather extended range of corrugations b, the model system exists in a two-phase state, in which commensurate patches coexist with incommensurate ones. (The term 'two-phase' refers here to inhomogeneities on a local scale and does not necessarily imply macroscopic phase separation.)

Depending on b, the structure of the system in the transition region varied from small do-

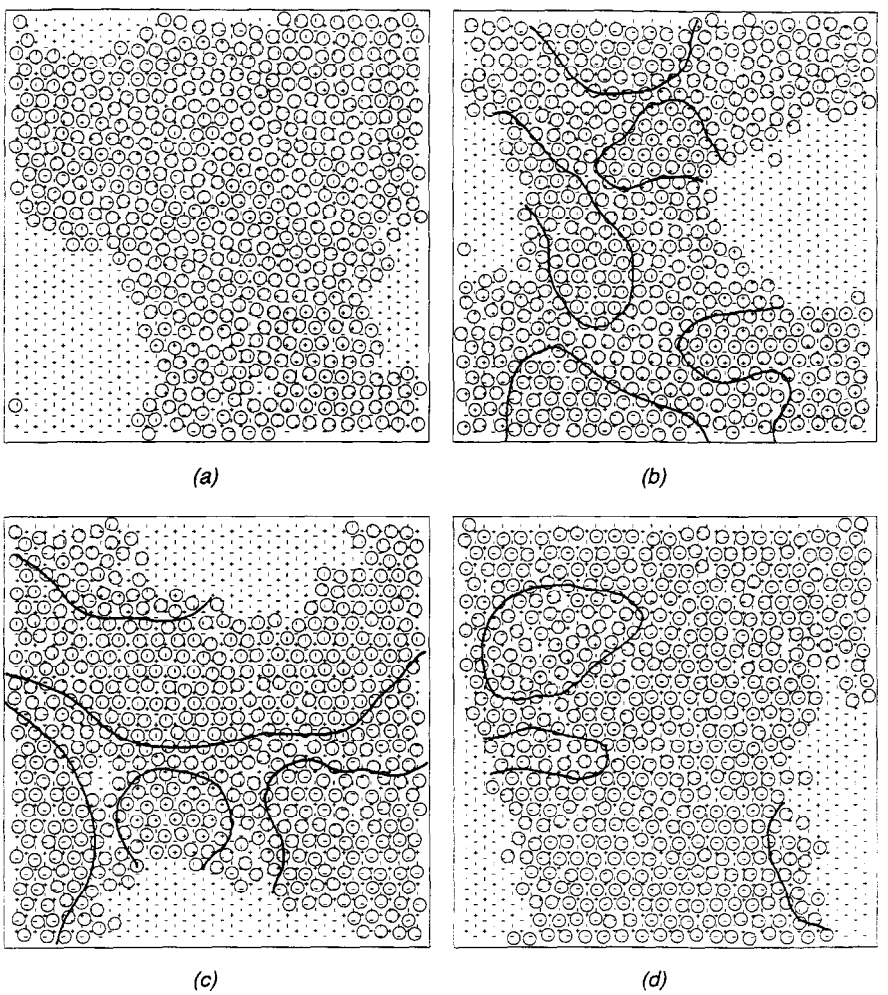

Fig. 3. Snapshots of the model 1 system at $T = 0.32$ and $A = 1.47$, for a corrugation b equal to (a) 0.1, (b) 0.2, (c) 0.26, and (d) 0.3. The adsorbate particles are shown as circles, while the potential adsorption sites on the substrate surface as dashes, sticks, and crosses. The adsorption sites belonging to the same $(\sqrt{3} \times \sqrt{3})R30°$ sublattice are marked by the same symbol. Encircled are patches of the substrate-modulated local ordering.

mains of substrate-modulated order in an incommensurate crystalline matrix (Fig. 3b) to fairly extended commensurate areas separated by disordered walls (Fig. 3c) and then to small patches of disorder in a commensurate crystalline environment (Fig. 3d). The exact boundaries of the transition region were however difficult to locate because of ambiguity involved in the definition of pure commensurate and pure incommensurate structures in terms of s. In the T–b phase diagram presented in Fig. 1, the transition region is shown as a shaded area whose boundaries were chosen, somewhat arbitrarily, based on a visual analysis of the relevant snapshots. Also indicated in the T–b diagram is an S_i–S_c boundary separating 'preferentially incommensurate' and 'preferentially commensurate' phase states. The boundary state was assumed to be the one in which the two component peaks in the distribution of s were nearly equal in intensity and the r.m.s. fluctuation $\sigma(s)$ was a maximum.

For one selected value of the surface corrugation, $b = 0.4$, we have mapped out the entire T–A phase diagram of the model system. In this diagram shown in Fig. 4 one can see the presence of the same five regions as in the T–b diagram (Fig. 1). At high densities (smaller A), the system forms an incommensurate solid phase S_i. As the density is decreased, this phase either melts or transforms into a commensurate solid in exactly the same (continuous) way as illustrated in Figs. 2 and 3 for the case of variable b. It is important that the S_i–S_c boundary in Fig. 4 is at an angle to the temperature axis, so that the loss of commensurability may be induced by increasing both the coverage at a fixed temperature and the temperature at a fixed coverage. At yet lower densities, a gas phase makes its appearance and the system enters two-phase regions. To illustrate the effect of b on the S_i–S_c phase transition, Fig. 4 shows, as a dashed line, the position of the S_i–S_c phase boundary for $b = 0.3$.

The calculated phase diagrams in Figs. 1 and 4 show what can be expected to happen to the assembly of the headgroups in $C_nS/Au(111)$ SAMs on variation of the substrate surface corrugation, temperature, and coverage. Qualitatively, the transformations predicted do not contradict the little what is known about the phase behavior of these monolayer systems. The most

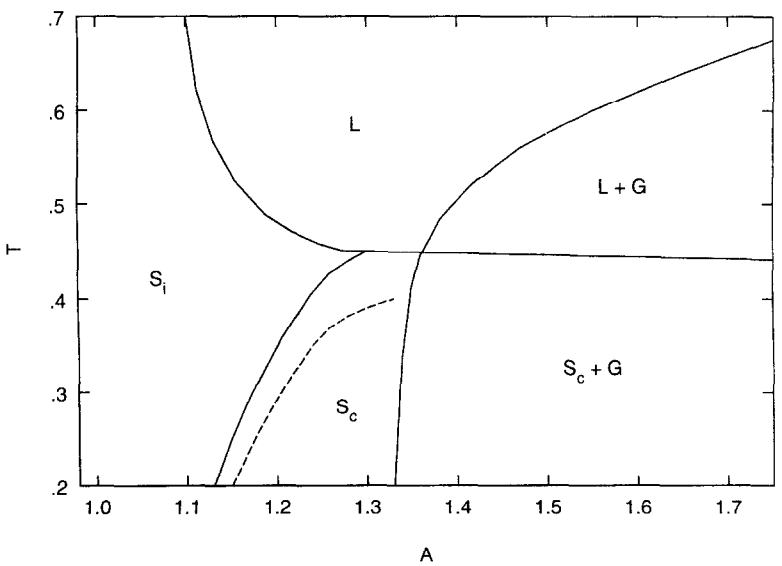

Fig. 4. The T–A phase diagram of the model 1 system for $b = 0.4$. The dashed line indicates the position of the S_i–S_c phase boundary for $b = 0.3$.

interesting prediction is the existence of a two-phase premelting region in which a commensurate ordered phase coexists with an incommensurate one. For smaller values of b, which formally correspond to long-chain alkanethiols (because $b = b_{abs}/\varepsilon$ and ε is nearly proportional to the chain length n), the incommensurate phase retains a crystal-like order (Fig. 3b), so that two different crystal phases coexist. The reasonableness of this result is supported by the temperature behavior of the grazing incidence X-ray diffraction pattern from long-chain ($n \geq 14$) $C_nS/Au(111)$ SAMs, as reported by Fenter et al. [2] In has been found that the loss of commensurability occurs in a wide temperature range and is accompanied by broadening and splitting of the diffraction peaks. This observation provides strong evidence for the coexistence of two solid phases with similar lattice spacings, as it occurs in Fig. 3b.

For larger values of b, which formally correspond to shorter alkane chains, the model predicts coexistence of ordered commensurate and disordered incommensurate regions (Fig. 3c, d). This is again in agreement with the observations of Fenter et al. [2], who found that short-chain ($n \leq 12$) $C_nS/Au(111)$ SAMs do not experience the commensurate–incommensurate solid-phase transition, but show a premelting region in which the commensurate crystalline phase coexists with a disordered one. whilst Fenter et al. [2] interpret this state in terms of solid–liquid coexistence, it is equally reasonable to associate the appearance of disordered patches with a gradual loss of commensurability due to the S_c–S_i solid phase transition.

Now we turn to model 2. The phase behavior of the system of two-center particles was studied as a function of temperature at $b = 0$ along the isochore $A = 1.3$ and at $b = 0.5$ along the isochores $A = 1.3$ and 1.6. In the case of a substrate-free monolayer ($b = 0$), an unexpected result was that the molecules proved to be tilted at $\varepsilon_z = 0$, when the tail-substrate attraction was switched off. The mean value of the tilt angle was about 30° at $T = 0.25$ and decreased monotonously with temperature down to 13° at $T = 0.5$. The result that the molecules prefer to

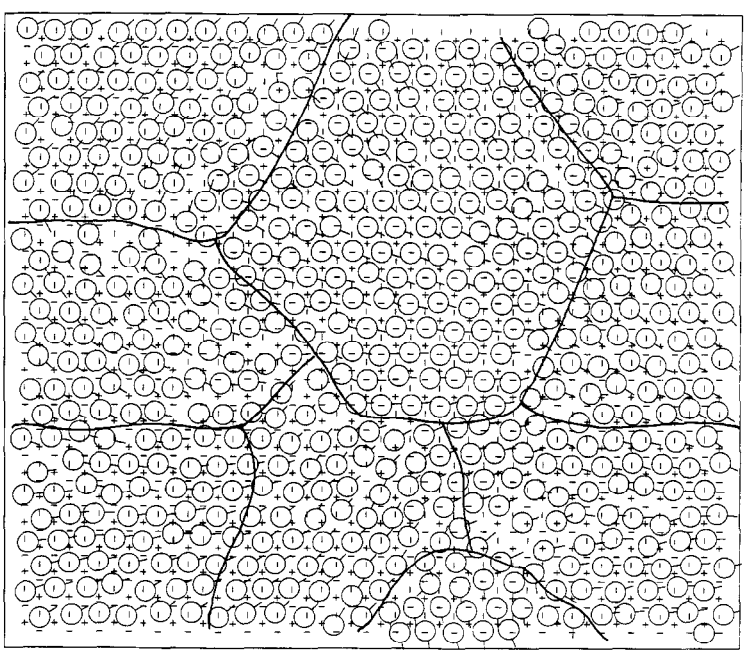

Fig. 5. A snapshot of the model 2 system at $T = 0.25$ and $A = 1.3$ showing domain structure of the commensurate solid. For clarity, the molecular tails are depicted about 3 times shorter than their actual projections onto the substrate surface.

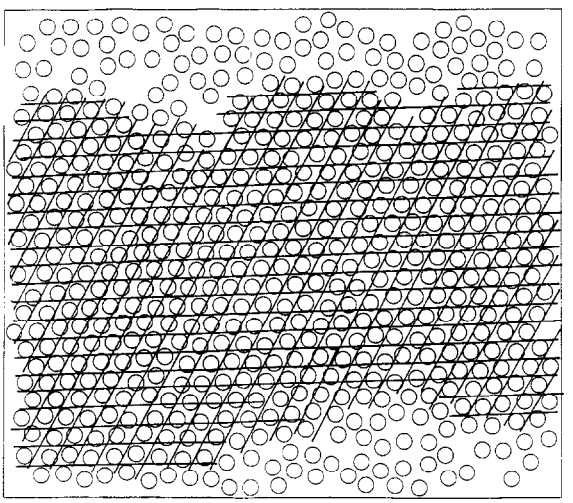

Fig. 6. A snapshot of the model 2 system at $T = 0.32$ and $A = 1.3$ illustrating long-range order in the arrangement of molecular centers in the incommensurate solid. (The thin parallel lines are a guide to eye, showing long-range translational order).

tilt even on an absolutely smooth substrate is contrary to the commonly accepted view that the origin of the tilt is the tendency of the molecules to accommodate the substrate lattice while retaining the close packing of the chains. Our simulations of the substrate-free monolayer showed that the reason of the tilt is rather the trend of the admolecules to spread over the whole surface area. The driving force behind this trend is to avoid an energy loss due to the molecules which are located at the monolayer edges and are short of neighbors.

At $b = 0.5$ and $A = 1.3$, the phase behavior of the model 2 system was similar to that discussed above for model 1. At low temperatures, the two-center molecules formed a commensurate $(\sqrt{3} \times \sqrt{3})R30°$ solid phase, as exemplified in Fig. 5 for $T = 0.25$. One can see

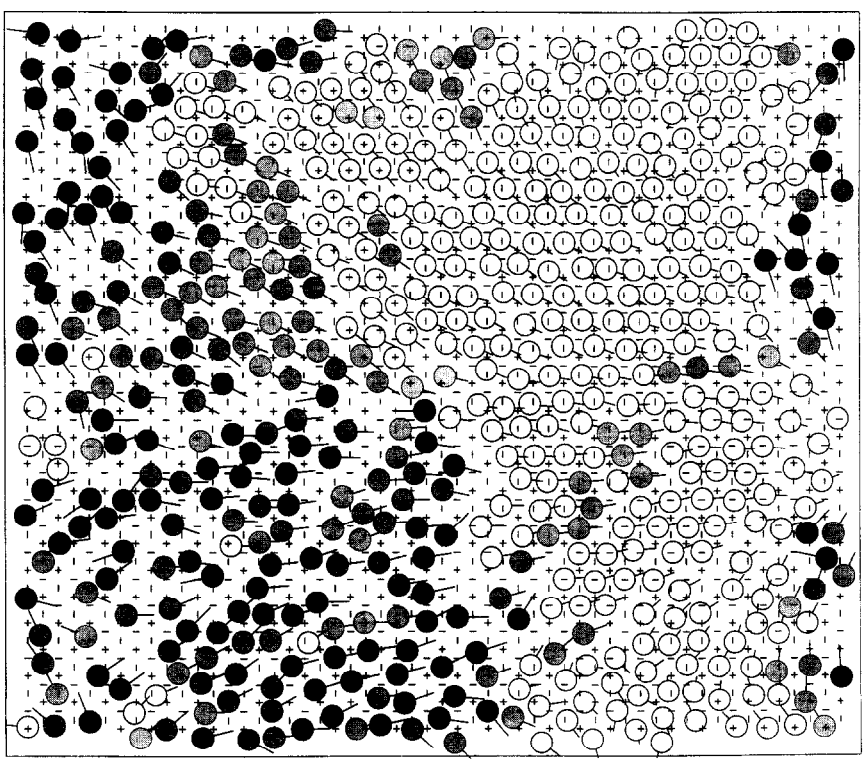

Fig. 7. A snapshot of the model 2 system at $T = 0.25$ and $A = 1.6$ showing a typical two-phase structure. Molecules tilted by more than 37° are depicted shaded, with the shading intensity proportional to the tilt angle. The darkest molecules lie parallel to the substrate surface.

well-defined domains, in which the constituent molecules have similar tilt directions and occupy the same subsystem of the adsorption sites. With increasing temperature, the coherence between the assembly of the headgroups and the substrate lattice worsened until the system transformed into an incommensurate solid at $T = 0.30–0.32$. A relevant snapshot (Fig. 6) shows a clear translational long-range order in the arrangement of the molecular centers. At $T = 0.32$, the incommensurate lattice spacing was found to be 1.05, which is perceptibly smaller than the substrate-dictated value 1.14. The melting of the $b = 0.5$ system was observed at $T = 0.35$. A remarkable feature of the melt was that the molecules retained an order in tilt directions, even though the long-range translational order had been completely lost. (In this respect, the system was similar to liquid crystals). This simulation result is opposite to what was observed in the atomistic simulation of an $N = 90$ system [6], which lost orientational order *before* melting. The exaggerated stability of the atomistic $N = 90$ system [6] toward melting was most likely due to extra periodicity imposed upon the system by periodic boundary conditions in combination with a small system size.

At $A = 1.6$, which corresponds to about 77% of the highest possible occupancy of the available adsorption sites, the model 2 system showed an unusual two-phase coexistence state. A relevant snapshot of the system is depicted in Fig. 7. One phase represents the usual commensurate solid constituted by molecules with 'normal' tilt angles ($\sim 30°$). The other phase is translationally disordered (liquid-like) and characterized by anomalously large tilts of its constituent molecules. (Some of the molecules in this disordered phase have even fallen and lie parallel to the substrate surface). The driving force for the formation of this unusual phase is again the trend of the system to occupy as large an area as possible, so as to avoid edge effects.

The failure of model 2 to predict the 'striped' structure for the low-density phase can result from, at least, two flaws in the forcefield used. First, it appears that the linear alkanethiol dimers observed in the striped phase have their origin in the formation of disulfide bonds between alkanethiol molecules [16]. Hence, the model forcefield should include a term (e.g., a Morse potential) responsible for such bonds. The second flaw of the model 2 forcefield is that Eq. (6) for the potential well depth does not distinguish between the side-by-side and end-to-end parallel configurations: $\varepsilon = 1$ for both. This flaw has been removed by Gay and Berne [13] by introducing an additional orientation-dependent factor into the equation for ε. A comparison of the resulting potential with the atom–atom potential for two $C_{10}S$ molecules showed, however, that the former provides a too strong orientation dependence and can hardly be used in describing $C_nS/Au(111)$ SAMs. A search for appropriate modifications of model 2 so as to simulate the striped phase will be the subject of our future work.

Acknowledgements

This work was supported by DFG through Sonderforschungsbereich 359. MG thanks the Deutsche Forschungsgemeinschaft and the DAAD for supporting a sabbatical leave and a travel grant.

References

[1] A. Ulman, An Introduction to Thin Organic Films: From Langmuir–Blodgett to Self-Assembly (Academic Press, Boston, MA, 1991), M. Grunze, Phys. Scr. 7 (1993) 711, N. Camilone III, C.E.D. Chidsey, G.-Y. Liu and G. Scoles, J. Chem. Phys. 98 (1993) 3503; E. Delamarche, B. Michel, Ch. Gerber, D. Anselmetti, H.-J. Guentherodt, H. Wolf and H. Ringsdorf, Langmuir 10 (1994) 2869; G.E. Poirier and M.J. Tarlov, Langmuir 10 (1994) 2853; G.-Y. Liu and M.B. Salmeron, Langmuir 10 (1994) 367.

[2] P. Fenter, P. Eisenberger and K.S. Liang, Phys. Rev. Lett. 70 (1993) 2447.

[3] G.E. Poirier, M.J. Tarlov and H.E. Rushmeier, Langmuir 10 (1994) 2853.

[4] G.E. Poirier and E.D. Pylant, Science 272 (1996) 1154.

[5] A.J. Pertsin and M. Grunze, Langmuir 10 (1994) 3668.

[6] J. Hautman, M.L. Klein, J. Chem. Phys. 93 (1990) 7483.
[7] J. Hautman, M.L. Klein, J. Chem. Phys. 91 (1989) 4994; J. Hautman, J.P. Bareman, W. Mar and M.L. Klein, J. Chem. Soc. Faraday Trans. 87 (1991) 2031; W. Mar and M.L. Klein, Langmuir 10 (1994) 188; J.I. Siepmann and I.R. McDonald, Mol. Phys. 2 (1992) 255.
[8] J.I. Siepmann and I.R. McDonald, Langmuir 9 (1993) 2351.
[9] A.J. Pertsin and A.I. Kitaigorodsky, The Atom–Atom Potential Method, Springer, Berlin, 1987.
[10] W.W. Wood, in: H.N.V. Temperley, J.S. Rowlinson and G.S. Rushbrooke (Eds.), Physics of Simple Liquids, North Holland, Amsterdam, 1968, p. 115.
[11] C. Taut, A.J. Pertsin and M. Grunze, Langmuir (1996), accepted.
[12] B.J. Berne and P. Pechukas, J. Chem. Phys. 56 (1972) 4213.
[13] J.G. Gay and B.J. Berne, J. Chem. Phys. 74 (1981) 3316.
[14] K.J. Strandburg, Rev. Mod. Phys. 60 (1988) 161.
[15] M.P. Allen and D.J. Tildesley, Computer Simulation of Liquids, Clarendon Press, Oxford, 1987.
[16] P. Fenter, A. Eberhardt and P. Eisenberger, Science 266 (1994) 1216.